it is only 11%; this difference may be due to the different way the primary particles are linked through the vanadium-containing surface species. The results obtained with the samples calcined at 973 K (through impregnation or through melting) are practically coincident in these two sets of samples (silica- and alumina-supported), as melting of the supported phase will probably lead to a very effective blocking of the mesopores and a "decoration" of the primary particles of the support with some sort of vanadia film that will behave also as an adhesive agent, thus soldering the primary particles of the support.

The results obtained with the rutile-supported samples are quite different from those with the silica- and the alumina-supported samples. First of all, the support itself reduces its specific surface area by calcination at 973 K (see Table I, samples T-773 and T-973), and the S_{BET} values for the rutile-supported samples obtained by impregnation are fairly close to those for the unloaded support submitted to calcination at the same temperatures. However, larger S_{BET} decreases are found for samples corresponding to series M, than with those corresponding to series I, despite the vanadium content being the same, Figure 4 (8.6 and 4.1 $m^2 g^{-1}$, respectively, for samples T-I-973-2 and T-M-973-2). It seems that the method of vanadium incorporation (impregnation or melting) still has an effect on the sintering/agglomeration process taking place during melting of vanadia; if vanadium has been incorporated via impregnation, the specific surface area is ca. twice, even after heating at 973 K, the value for the sample where the vanadium has been incorporated by melting, having the same vanadium content (3.4%) and having been calcined at the same temperature (973 K).

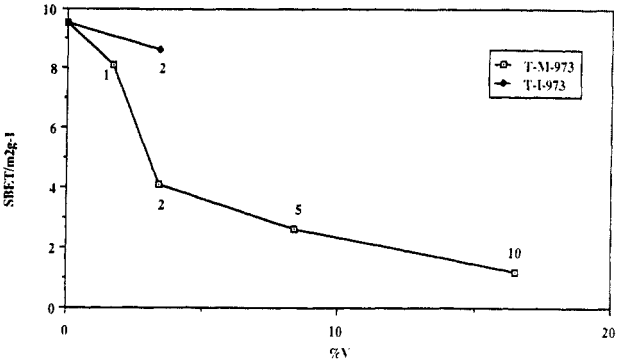

Figure 4. Variation in the specific surface area of samples prepared on rutile with the vanadium content (labels correspond to the number of monolayers of V_2O_5).

Acknowledgment. Thanks are given to CICYT (Grant MAT88-0556) and Junta de Castilla y León for finantial support. Gift of the oxide samples is also acknowledged.

Registry No. V_2O_5, 1314-62-1; TiO_2, 13463-67-7.

Ethylidyne on the Rh(100) Surface: A Theoretical Investigation

Birgit Schiøtt† and Roald Hoffmann*

Department of Chemistry and Materials Science Center, Cornell University, Ithaca, New York 14853-1301

Mohamed K. Awad and Alfred B. Anderson

Chemistry Department, Case Western Reserve University Cleveland, Ohio 44106

Received July 26, 1989. In Final Form: November 17, 1989

The bonding of ethylidyne (CCH_3) on the Rh(100) surface is analyzed by using the extended Hückel tight-binding approach and also the ASED-MO theory with cluster models. The relative stabilities for ethylidyne bound at the on-top, bridging, and the 4-fold hollow sites of Rh(100) are discussed and compared with the well-characterized geometry of ethylidyne in the 3-fold hollow site of the Rh(111) surface. The theoretical indicators of bonding support the experimental assignment of a 4-fold hollow site for CCH_3. In this geometry, the e orbitals of ethylidyne interact most with the surface, resulting in a better rhodium–carbon bond and a stronger carbon–carbon bond. A comparison is made between the bonding of ethylidyne to discrete transition-metal fragments and to the Rh(100) and Rh(111) surfaces. A 4-fold site certainly has the appropriate orbitals to bind strongly a CR fragment.

Carbyne ligands are well-known ligands in organometallic chemistry.[1] The first compounds of this class to be synthesized and characterized were $XM(CO)_4(CR)$ (X = Cl, I, Br; M = Cr, Mo, W; R = CH_3, C_6H_5), 1, made by Fischer and co-workers in 1973.[2]

† Permanent address: Department of Chemistry, University of Århus DK-8000 Århus C, Denmark.

(1) (a) Fischer, E. O.; Schubert, U. *J. Organomet. Chem.* **1975**, *100*, 59. (b) Schrock, R. R. *Acc. Chem. Res.* **1986**, *19*, 342. (c) Nugent, W. A.; Mayer, J. M. *Metal-ligand Multiple Bonds*; Wiley: New York, 1988.

0743-7463/90/2406-0806$02.50/0

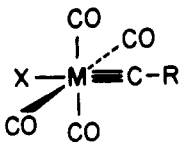

1

Several X-ray structures of complexes with an ethylidyne (CCH_3) ligand, the subject of this paper, bound η^1 (monohapto, terminally), have now been published.[3] All terminal ethylidyne complexes are with group IVA transition metals,[1c] such as **1**, whereas several terminal alkylidyne compounds have been made with other metals, such as Ta, Mn, Re, Fe, and Os.[4] Two compounds have been determined where ethylidyne bridges two transition-metal centers,[5] as exemplified by **2**. A large number of trinuclear compounds, such as **3** (carbonyls are not drawn), with ethylidyne bridging all three metals are known.[5c,6] Even the existence of a compound with ethylidyne bridging four metals has been reported.[7] To our knowledge, in all multinuclear complexes the ethylidyne fragment bridges as many metal atoms as possible. For instance, it is known that the terminally bound ethylidyne in $WCl(CO)_4(CCH_3)$ becomes bridging as soon as other metals are present[5a] and that AgCl added to $Os(CR)(Cl)(CO)(PPh_3)_2$ leads to a complex where the alkylidyne ligand bridges the Os atom and the Ag atom.[8]

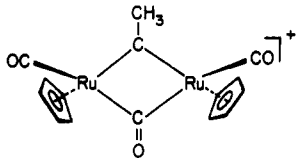

2

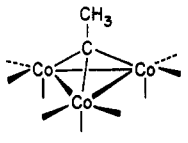

3

During the last decade, it has become evident that the ethylidyne fragment is also a common surface species. It is, for instance, formed as a "byproduct", strongly bound to the surface, in the hydrogenation of ethylene to ethane on various late-transition-metal surfaces.[9] The overall reaction rate for ethane production is not influenced by the existence of this fragment on the surface—it plays a "spectator" role.[9c,d,10] Ethylidyne is also the stable species found at room temperature on various acetylene and ethylene exposed surfaces.[11] At lower temperatures (below 200 K), acetylene adsorbs on the Pt(111) surface with the carbon–carbon bond parallel to the surface layer, with its two hydrogens bent away form the surface.[11a] Upon heating to room temperature, the acetylene rearranges to an ethylidyne.[11a] This transformation is thought to pass via a vinylidene (CCH_2) species,[12] but the rearrangement is not at all well understood. The mechanism for the rearrangement of ethylene to ethylidyne is also disputed in the literature.[13] It has been suggested, on theoretical grounds, that an initial dehydrogenation to a vinyl fragment ($CHCH_2$), followed by reaction to ethylidene ($CHCH_3$) and ethylidyne (CCH_3), is the energetically favored reaction path.[9d,14] In a very recent paper, White et al.[13] show that an adsorbed ethyl fragment (coadsorbed with Cl from a photodissociation of C_2H_5Cl on Pt(111)) rearranges to di-σ-bound ethylene, which then transforms to ethylidyne. This seems to exclude ethyl (CH_2CH_3) as an intermediate. The fragments ethylidene[15] and vinyl[16] have been identified as intermediates in the transformation of ethylene to ethylidyne.

Ethylidyne has been characterized on many close-packed fcc surfaces, such as Ir(111),[11f] Pt(111),[11b,h] Rh(111),[11a,c] Ni(111),[11g] and Pd(111)[11d,e] as well as on the hexagonal Ru(001) surface.[17] From various pieces of experimental evidence, it has become clear that ethylidyne sits in the 3-fold hollow site of the fcc(111) surfaces.[11] Theoretically, this observation has been rationalized by our group[18] and by others.[9d,14,19] The ethylidyne fragment has been shown to take an upright position with the carbon–carbon bond perpendicular to the surface,[11] **4**.

(2) Fischer, E. O.; Kreis, G.; Kreiter, C. G.; Müller, J.; Huttner, G.; Lorenz, H. *Angew. Chem., Int. Ed. Engl.* **1973**, *12*, 564.
(3) (a) Krüger, C.; Goddard, R.; Claus, K. H. *Z. Naturforsch.* **1983**, *38B*, 1431. (b) Huttner, G.; Lorenz, H.; Gartzke, W. *Angew. Chem.* **1974**, *86*, 667. (c) Huttner, G.; Frank, A.; Fischer, E. O. *Isr. J. Chem.* **1977**, *15*, 133. (d) Chice, K. W.; Jones, R. A.; Wilkinson, G.; Gales, A. M. R.; Hursthouse, M. B.; Malik, K. M. A. *J. Chem. Soc., Dalton Trans.* **1981**, 1204. (e) Chisholm, M. H.; Hoffman, D. M.; Huffman, J. C. *Inorg. Chem.* **1983**, *22*, 2903.
(4) (a) Ta compounds: Churchill, M. R.; Wasserman, H. J.; Schrock, R. R. *J. Am. Chem. Soc.* **1982**, *104*, 1710. Churchill, M. R.; Youngs, W. J. *Inorg. Chem.* **1979**, *18*, 171. Guggenberger, L. J.; Schrock, R. R. *J. Am. Chem. Soc.* **1975**, *97*, 2935. (b) Mn compounds: Kolobova, N. E.; Ivanov, L. L.; Zhvanko, O. S.; Khitrova, O. M.; Batsanov, A. S.; Struchkov, Yu. T. *J. Organomet. Chem.* **1984**, *262*, 39. (c) Re compounds: Edwards, D. S.; Biondi, L. V.; Ziller, J. W.; Churchill, M. R.; Schrock, R. R. *Organometallics* **1983**, *2*, 1505. Savage, P. D.; Wilkinson, G.; Motewalli, M.; Hursthouse, M. B. *Polyhedron* **1987**, *6*, 1599. Pombeiro, A. J. L.; Hughs, D. L.; Pickett, C. J.; Richards, R. L. *J. Chem. Soc., Chem. Commun.* **1986**, 246. Pombeiro, A. J. L.; Carvalho, M. F. N. N.; Hitchcock, P. B.; Richards, R. L. *J. Chem. Soc., Dalton Trans.* **1981**, 1629. (d) Fe compounds: Fischer, E. O.; Schneider, J.; Neugebauer, D. *Angew. Chem., Int. Ed. Engl.* **1984**, *23*, 820. (e) Os compounds: Roper, W. R. *J. Organomet. Chem.* **1986**, *300*, 167. Clark, G. R.; Edmonds, N. R.; Pauptit, R. A.; Roper, W. R.; Waters, J. M.; Wright, A. H. *J. Organomet. Chem.* **1983**, *244*, C57. Clark, G. R.; Marsden, K.; Roper, W. R.; Wright, L. J. *J. Am. Chem. Soc.* **1980**, *102*, 6570.
(5) (a) Ashworth, T. V.; Howard, J. A. K.; Stone, F. G. A. *J. Chem. Soc., Dalton Trans.* **1980**, 1609. (b) Davies, D. L.; Dyke, A. F.; Endesfelder, A.; Knox, S. A. R.; Naish, P. J.; Orpen, A. G.; Plaas, D.; Taylor, G. E. *J. Organomet. Chem.* **1980**, *198*, C43. (c) Evans, J.; McNulty, G. S. *J. Chem. Soc., Dalton Trans.* **1984**, 79.
(6) (a) Skinner, P.; Howard, M. W.; Oxton, I. A.; Kettle, S. F. A.; Powell, D. B.; Sheppard, N. *J. Chem. Soc., Faraday Trans.* **1981**, *77*, 1203. (b) Sutton, P. W.; Dahl, L. F. *J. Am. Chem. Soc.* **1967**, *89*, 261.
(7) Eady, C. R.; Fernandez, J. M.; Johnson, B. F. G.; Lewis, J.; Raithby, P. R.; Sheldrick, G. M. *J. Chem. Soc., Chem. Commun.* **1978**, 421.
(8) Clark, G. R.; Cochrane, C. M.; Marsden, K.; Roper, W. R.; Wright, L. J. *J. Organomet. Chem.* **1986**, *315*, 211.
(9) (a) Zaera, F.; Somorjai, G. A. *J. Am. Chem. Soc.* **1984**, *106*, 2288. (b) Godbey, D.; Zaera, F.; Yeates, R.; Somorjai, G. A. *Surf. Sci.* **1986**, *167*, 150. (c) Somorjai, G. A.; Van Hove, M. A.; Bent, B. E. *J. Phys. Chem.* **1988**, *92*, 973. (d) Anderson, A. B., Choe, S. J. *J. Phys. Chem.* **1989**, *93*, 6145.
(10) Beebe, T. P., Jr.; Yates, J. T., Jr. *J. Am. Chem. Soc.* **1986**, *108*, 663.
(11) (a) Koestner, R. J.; Van Hove, M. A.; Somorjai, G. A. *Surf. Sci.* **1982**, *121*, 321; *J. Phys. Chem.* **1983**, *87*, 203. (b) Kesmodel, L. L.; Dubois, L. H.; Somorjai, G. A. *J. Chem. Phys.* **1979**, *70*, 2180. (c) Koel, B. E.; Bent, B. E.; Somorjai, G. A. *Surf. Sci.* **1984**, *146*, 211. (d) Gates, J. A.; Kesmodel, L. L. *Surf. Sci.* **1981**, *111*, L474; **1982**, *120*, L461; **1983**, *124*, 68. (e) Kesmodel, L. L.; Waddill, D. W.; Gates, J. A. *Surf. Sci.* **1984**, *138*, 464. (f) Marinova, Ts. S.; Kostov, K. L. *Surf. Sci.* **1987**, *181*, 573. Marinova, Ts. S.; Chakarov, D. V. *Surf. Sci.* **1988**, *200*, 309. (g) Zhu, X.-Y.; White, J. M. *Surf. Sci.* **1989**, *214*, 240. (h) Stöhr, J.; Sette, F.; Johnson, A. L. *Phys. Rev. Lett.* **1984**, *53*, 1684. (i) Horsley, J. A.; Koestner, R. J. *J. Chem. Phys.* **1985**, *83*, 3146.
(12) (a) Ibach, H.; Lehwald, S. *J. Vac. Sci. Technol.* **1978**, *15*, 407. (b) Wang, P.-K.; Slichter, C. P.; Sinfelt, J. P. *Phys. Rev. Lett.* **1984**, *53*, 81.
(13) Lloyd, K. G.; Campion, A.; White, J. M. *Catal. Lett.* **1989**, *2*, 105.
(14) Kang, D. B.; Anderson, A. B. *Surf. Sci.* **1985**, *155*, 639.
(15) Zhou, X.-L.; Zhu, X.-Y.; White, J. M. *Surf. Sci.* **1988**, *193*, 387.
(16) See ref 13 and ref 27 therein.
(17) (a) Hills, M. M.; Parmeter, J. E.; Mullins, C. B.; Weinberg, W. H. *J. Am. Chem. Soc.* **1986**, *108*, 3554. (b) Parmeter, J. E.; Hills, M. M.; Weinberg, W. H. *J. Am. Chem. Soc.* **1986**, *108*, 3563.
(18) Silvestre, J.; Hoffmann, R. *Langmuir* **1985**, *1*, 621.
(19) Gavezzotti, A.; Simonetta, M. *Surf. Sci.* **1980**, *99*, 453.

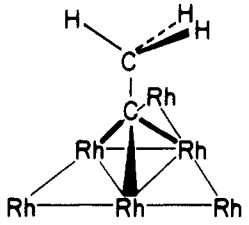

4

The carbon–carbon bond length of ethylidyne adsorbed on Pt(111)[11b] has been determined by LEED (low-energy electron diffraction) experiments to be 1.50 Å and on Rh(111)[11a] to be 1.45 Å. These structural findings suggest an ethane-like molecule, composed of two sp^3-hybridized carbons and a carbon–carbon single bond.[20]

Until recently, the ethylidyne fragment was identified only on surfaces with 3-fold hollow sites. Somorjai and co-workers report in two new papers[21] that they, from HREELS (high-resolution electron energy loss spectroscopy) experiments, have identified the formation of ethylidyne on the Rh(100) surface, which does not have any 3-fold hollow sites available. Reconstruction of the Rh(100) surface to a surface geometry with pseudo 3-fold hollow sites is unlikely to take place.[21a] This is the first time ethylidyne has been observed on a nonreconstructed (100) surface of a face-centered-cubic metal. Earlier studies of ethylene on Pd(100) gave $CHCH_2$[22] as the first stable (detectable) surface species, with no sign of ethylidyne at all. A definite assignment of the adsorption site for ethylidyne on Rh(100) could not be made, although it was shown that the carbon–carbon axis of ethylidyne is perpendicular to the surface plane.[21a] Somorjai and co-workers assigned a loss peak at 1015 cm^{-1} in the HREEL spectrum for ethylidyne adsorbed on Rh(100) to a carbon–carbon stretching frequency. For ethylidyne-covered Rh(111), this bond is characterized by a loss peak of 1120 cm^{-1}.[11c] Unfortunately, no IR data exist for terminal or 4-fold coordinated ethylidyne complexes. IR information is available for some of the 3-fold bridging ethylidyne complexes (the carbon–carbon stretching frequency varies from 1125 to 1163 cm^{-1}) and for **2** (1247 cm^{-1}).[5c] From these data, Somorjai and co-workers found it likely that an increase in coordination number for the ethylidyne will lead to a decrease in the carbon–carbon stretching frequency. They thus suggested that the 4-fold hollow site is the most likely one for ethylidyne on the Rh(100) surface.[21a]

In this study, we will look closer at how and where ethylidyne binds to the Rh(100) surface. The extended Hückel[23] tight-binding[24] approximation is used. Theoretical tools, such as the density of states (DOS),[25] projected density of states,[25] total energy, and crystal orbital overlap population (COOP),[25] will be used to make comparative judgements of preferred sites and bonding on the surface. Atom superposition and delocalization molecular orbital (ASED-MO) calculations[26] with cluster surface models have also been used. Results for ethylidyne adsorption on cluster models of the (111)Rh and (100)Rh surfaces are given. They are in general agreement with the extended Hückel band calculations.

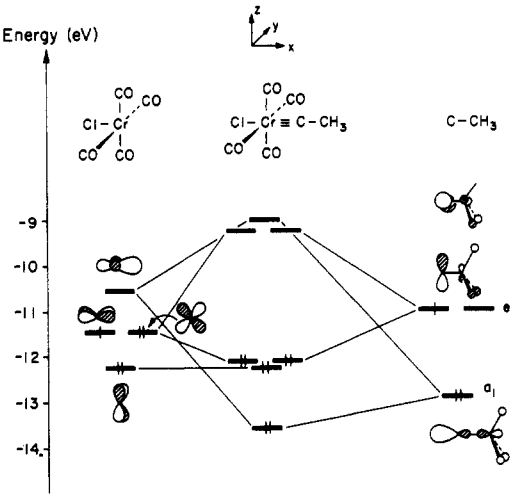

Figure 1. Orbital interaction diagram for the formation of $CrCl(CO)_4(CCH_3)$ from an ethylidyne fragment and a $CrCl(CO)_4$ fragment.

Bonding of Ethylidyne to Discrete Transition-Metal Fragments

Let us start with an analysis of the binding of ethylidyne to group IVA mononuclear complexes.[27a] $Cr(CO)_4(Cl)(CCH_3)$ is chosen as a model. The important frontier orbitals of ethylidyne are depicted in **5**, labeled according to their symmetry in C_{3v}.

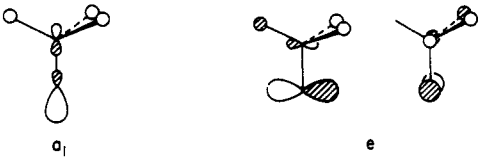

5

The a_1 orbital is moderately carbon–carbon bonding, but other lower lying orbitals also contribute to the formation of the carbon–carbon bond. The e orbitals, formally occupied by one electron, are carbon–carbon antibonding. An orbital interaction diagram, reduced to its essentials, is drawn in Figure 1 for the interaction between ethylidyne and the $Cr(CO)_4Cl$ fragment. Both fragments are considered neutral, leaving one electron in the e level and chromium in a formal oxidation state of +1, with five d electrons in the d block. Only the orbitals which interact strongest are shown in the figure. For the chromium fragment, outlined at the left-hand side of the figure, this means the well-known d orbitals of an ML_5 fragment.[27b] These are the four lowest orbitals of what were the t_{2g} and the e_g levels of a regular octahedral complex. The d_{z^2} orbital (not shown in the figure) is high up in energy, due to its strongly metal–ligand antibonding character. The other orbital from the octahe-

(20) It has been shown by ^{59}Co nuclear quadrupole resonance spectroscopy that through the apical carbon in $Co_3(CO)_9(CR)$ complexes a significant amount of π delocalization takes place in the clusters. Miller, D. C.; Brill, T. B. *Inorg. Chem.* **1978**, *17*, 240.

(21) (a) Slavin, A. J.; Bent, B. E.; Kao, C.-T.; Somorjai, G. A. *Surf. Sci.* **1988**, *202*, 388; (b) **1988**, *206*, 124.

(22) (a) Stuve, E. M.; Madix, R. J. *J. Phys. Chem.* **1985**, *89*, 105. (b) Stuve, E. M.; Madix, R. J.; Brundle, C. R. *Surf. Sci.* **1985**, *152*, 532.

(23) (a) Hoffmann, R. *J. Chem. Phys.* **1963**, *39*, 1397. (b) Hoffmann, R.; Lipscomb, W. N. *J. Chem. Phys.* **1962**, *37*, 2872.

(24) Whangbo, M.-H.; Hoffmann, R. *J. Am. Chem. Soc.* **1978**, *100*, 6093.

(25) (a) Hoffmann, R. *Solids and Surfaces. A Chemist's View of Bonding in Extended Structures*; VCH Publishers: New York, 1988. (b) Hoffmann, R. *Rev. Mod. Phys.* **1988**, *60*, 601. (c) Hoffmann, R. *Angew. Chem., Int. Ed. Engl.* **1987**, *26*, 846.

(26) (a) Anderson, A. B. *J. Chem. Phys.* **1975**, *62*, 1187. (b) Anderson, A. B., Grimes, R. W., Hong, S. Y. *J. Phys. Chem.* **1987**, *91*, 4245.

(27) (a) For a general discussion of metal–ligand triple bonds, see ref 1c, Chapter 2. (b) Albright, T. A.; Burdett, J. K.; Whangbo, M.-H. *Orbital Interactions in Chemistry*; Wiley: New York, 1985.

dral e_g set, the $d_{x^2-y^2}$ orbital, is stabilized considerably on going from ML_6 to ML_5, because of the removal of one of the antibonding metal–ligand interactions.[27b] Furthermore, it mixes in some s and p_x character, making it a really good acceptor orbital for interaction with a new ligand, here through the ethylidyne a_1 orbital. The orbitals that made up the t_{2g} set in ML_6 are only affected a little by going to ML_5.[27b] The d_{xz} and the d_{xy} orbitals are still degenerate, with the d_{yz} orbital located a little lower in energy. The d_{xz} and d_{xy} orbitals of $Cr(CO)_4Cl$ interact strongly with the e set of ethylidyne. No ethylidyne orbital has the right symmetry to interact with d_{yz}, and it stays unchanged. The three bonds traditionally drawn between a metal and a CR–ligand[1-3] originate in this model from a complete filling of the σ type bonding orbital, **6**, and the two π bonding orbitals, **7**.

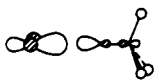

6

7

The bonding of ethylidyne to multinuclear compounds follows the same pattern, in that the bonds are made up from interactions of the a_1 and the e orbitals of ethylidyne with cluster orbitals of the appropriate symmetry. Some of the resulting bonding interactions are depicted in **8** for the 2-fold bridging complex, $Ru_2(Cp)_2(CO)_2(\mu^2\text{-}CO)(\mu^2\text{-}CCH_3)^+$, and in **9** for a trinuclear complex, such as $Co_3(CO)_9(\mu^3\text{-}CCH_3)$ and $M_3H_3(CO)(\mu^3\text{-}CCH_3)$, (M = Os, Ru).[28]

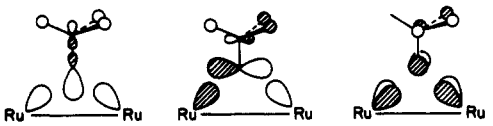

8

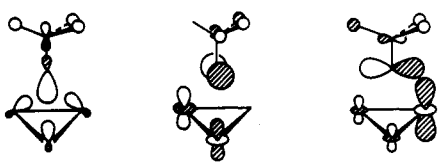

9

In the Os_6 cluster, where ethylidyne bridges four osmium atoms, **10** (in which a μ^3-ethylidyne is also found), molecular orbitals of appropriate symmetry for interaction with the a_1 and the e orbitals of ethylidyne exist. These interactions lead to semilocalized orbitals, which are responsible for the formation of the four osmium–carbon bonds.

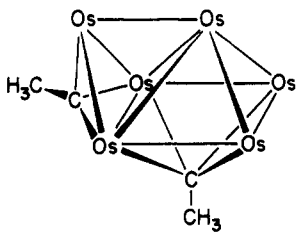

10

Thinking now of ethylidyne bound to a surface, whether it is on-top, bridging, in the 3-fold hollow site of Rh(111), or in the 4-fold hollow site of Rh(100), we expect that interactions relevant for each adsorption geometry take place. Whether they lead to a favorable bonding situation or not is determined by a combination of two factors: (i) where the Fermi level cuts the bands and (ii) how effective each of the interactions described in **6–9** is.

Let us be a little more specific on how these two factors may work together to control the overall bonding picture. In the case of ethylidyne terminally bound to a mononuclear complex, Figure 1, we have seen that all the metal–carbon bonding orbitals are occupied and that all the antibonding orbitals are empty. This is the favorable situation for obtaining a strong bond between the two atoms. On a surface, the bonding relationships are not quite the same, and the position of the Fermi level is critical. Consider an ethylidyne molecule sitting on a surface. The a_1 and e levels interact with the metal and spread out into bands. The width of these bands is an indicator of the strength of the interaction. The stronger the interaction, the wider the band becomes.[25] The bottoms of the resulting bands consist of metal–ligand bonding orbitals and the top part of their antibonding counterparts. The Fermi level will cut these bands at a specific energy. Two extreme situations may obtain, indicated by arrows in **11**.

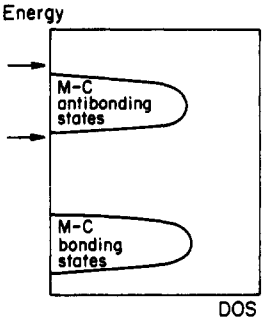

11

If the Fermi level cuts the band just below the antibonding peak (lower arrow), then one has a very good surface–adsorbate bond. The poor bond obtained in the second case (higher arrow) is a result of the Fermi energy being above the antibonding peak. Both metal–adsorbate bonding and antibonding states are then filled, with the consequence of little net bonding. In the following, we will distinguish between a good and a bad bonding situation by looking at the width of the interacting bands, mainly those of the frontier orbitals of ethylidyne, a_1 and e, and at the energy where the Fermi level cuts these bands.

Ethylidyne Adsorbed on Rh(100): Extended Hückel Band Results

Let us now proceed to the adsorbed system—ethylidyne on Rh(100). Somorjai and co-workers identified the ethylidyne on a Rh(100) surface coadsorbed with carbon monoxide, in a c(4×2) LEED pattern.[21a] The coverage of ethylidyne was 0.25.[21a] A coverage of 0.50 is used by us in order to avoid too large a unit cell. For an

(28) (a) Hoffman, D. M.; Hoffmann, R.; Fisel, C. R. *J. Am. Chem. Soc.* **1982**, *104*, 3858. (b) Sappa, E.; Tiripicchio, A.; Braunstein, P. *Chem. Rev.* **1983**, *83*, 203. (c) Schilling, B. E. R.; Hoffman, R. *J. Am. Chem. Soc.* **1979**, *101*, 3456.

ethylidyne coverage of 0.50, no significant ethylidyne–ethylidyne contacts are present.[29] A calculation for the full c(4×2) structure with CO coadsorbed, as proposed in ref 21a, was also performed. Very similar results are obtained for the two structures. Also, as a compromise between computation time and accuracy of the results, we have chosen a three-layer rhodium slab. Earlier work by our group has shown that this is a satisfactory compromise.[30]

Rhodium is a face-centered-cubic metal with a = 3.80 Å. The (100) surface presents a square net of rhodium atoms with a nearest neighbor distance of 2.69 Å. For 4-fold hollow site adsorbed ethylidyne, the unit cell is as depicted in 12.

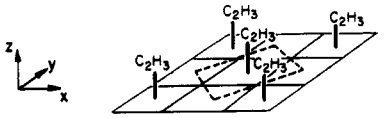

12

No bond lengths for the ethylidyne/Rh(100) system have been published. We assume a carbon–carbon distance of 1.45 Å, which is the separation reported from a LEED crystallographic investigation of ethylidyne adsorbed in the 3-fold hollow site of Rh(111).[11a] Because the 4-fold adsorption site for ethylidyne on Rh(100) is the one suggested experimentally, we will focus on this surface geometry and compare it to adsorption in the two other high-symmetry sites on Rh(100)—the on-top site and the 2-fold bridging site. We will also compare the bonding between ethylidyne and the Rh(100) surface with the bonding obtained for the well-characterized 3-fold bridging ethylidyne on Rh(111).

With the carbon–carbon bond length fixed at 1.45 Å, let us start out with an estimation of the rhodium–carbon distance. A minimum in the total energy is calculated to be at ~2.20 Å for an orientation of ethylidyne as shown from a top view in 13. The structure 14, obtained by turning the ethylidyne fragment by 15° so one C–H bond points directly above a surface rhodium atom, gives results very similar to those obtained for 13. The rotational barrier for CCH_3 in the 4-fold site is 12-fold, so one would not imagine a substantial barrier between the two conformations. It is in fact calculated to be ~0.01 eV. For the rest of the study, we will use 13 as a model for a 4-fold adsorbed ethylidyne.

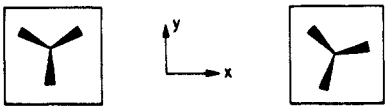

13 14

Extended Hückel calculations are typically not that reliable in predicting bond distances. To convince ourselves that for this system the method may not be too bad, we did a similar calculation for a 3-fold adsorbed ethylidyne on Rh(111). Here we found an energy minimum at a rhodium–carbon distance of 1.99 Å. The experimental value to compare with is 2.03 Å[11a]—so the agreement is pretty good. No organometallic clusters with ethylidyne bridging three rhodium atoms have been reported. For the $Co_3(CO)_9(\mu^3\text{-}CCH_3)$ structure, the metal–carbon distance is 1.90 Å,[6b] and for $H_3M(CO)_9(\mu^3\text{-}CCH_3)$ (M = Ru, Os), this distance is 2.08 Å.[11a] In the subsequent analysis, we work with a rhodium–carbon separation of 2.20 Å. The qualitative conclusions made from this study are not sensitive to this distance, but they apply as well, as we explored in some model calculations, for Rh–C distances in the range ~2.00 to ~2.30 Å.

The conformations shown in 15 are used for the three adsorption sites on Rh(100).

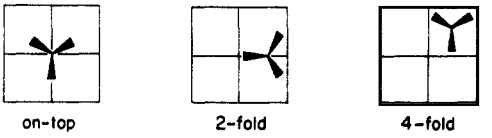

15

We kept the Rh–C distance fixed (2.20 Å), so that the perpendicular carbon–surface separation varied between the sites. Further details of the computations are given in the Appendix.

In Table I are listed some important results for these sites. The binding energies listed, ΔE, are defined in such a way that a positive number reflects an attractive interaction. We see that all three sites lead to a bonding situation and that the 4-fold site is stabilized by 0.3 and 0.1 eV relative to the on-top and the 2-fold bridging sites, respectively. The calculated Fermi level for a bare Rh(100) surface is −8.57 eV, much higher than the energy of the partly filled e orbitals (−10.9 eV). Most of the stabilization accompanying adsorption is due to charge transfer from the Fermi level of Rh(100) to the e orbitals of ethylidyne, as described in 16.

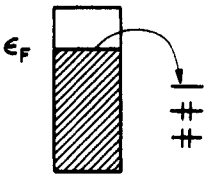

16

By viewing the process as an adsorption of a CCH_3^{3-} ion on a Rh(100) surface with a formal charge of +3 per unit cell, one can extract out the covalent part of the binding energy. These are tabulated as ΔE_{cov}. Again a positive value means attraction. Adsorption in any of the three sites also leads to a covalently stabilized system. The energy considerations give the 4-fold adsorption site as slightly more favorable.

The overlap populations listed concur; while the strongest single Rh–C bond is calculated for the on-top site, in the 2-fold bridging site and the 4-fold hollow site two, respectively, four relatively strong surface Rh–C bonds are present. A detailed analysis of the COOP curves provides us with some further insight into the site preference, as will be shown below.

Let us now discuss in some detail how ethylidyne, a fragment with C_{3v} symmetry, binds to the 4-fold hollow site of the square Rh(100) surface. In Table II we have listed changes in electron densities upon adsorption. Significant changes occur in most of the d orbitals. An electron flow from the surface layer to the ethylidyne fragment and to the bulk layers of the rhodium slab is calculated. The a_1 orbital of ethylidyne loses 0.31 electron,

(29) Nearest-neighbor distances are 2.69 Å between two methyl carbons (overlap population is calculated to be −0.001) and between two singly coordinated carbons (overlap population = 0.001). The closest H–H distance is 2.12 Å with a corresponding overlap population of 0.003.
(30) Saillard, J.-Y.; Hoffmann, R. *J. Am. Chem. Soc.* **1984**, *106*, 2006.

Table I. Binding Energies and Overlap Populations for Adsorption of Ethylidyne in Different Sites on Rh(100)

	on-top	2-fold	4-fold
energy			
ΔE,[a] eV	6.4	6.6	6.7
ΔE_{cov},[b] eV	0.2	0.4	0.5
overlap population			
C–C[c]	0.790	0.807	0.832
Rh–C	0.459	0.417	0.359
Rh–Rh[d]	0.214	0.123	0.147

[a] $\Delta E = E(\text{Rh(100)}) + E(CCH_3) - E(\text{adsorbed system})$. [b] $\Delta E_{cov} = E(\text{Rh(100)}^{3+}) + E(CCH_3^{3-}) - E(\text{adsorbed system})$. [c] C–C overlap population of a CCH_3 fragment is 0.962. [d] Overlap population between the two surface rhodiums nearest the adsorbed ethylidyne fragment. The surface rhodium to surface rhodium overlap population is 0.223 on a bare Rh(100) surface.

Table II. Electron Densities for a CCH_3 Fragment, a Clean Rh(100) Surface, and the 4-Fold Adsorbed System

	Rh(100) + CCH_3 separated	4-fold
surface rhodium		
$4d_{x^2-y^2}$	1.52	1.34
$4d_{z^2}$	1.86	1.79
$4d_{xy}$	1.79	1.60
$4d_{xz} + 4d_{yz}$	3.36	2.89
bulk rhodium[a]		
total	8.37	8.50
CCH_3		
a_1	2.00	1.69
e	1.00	2.75

[a] The bulk density is taken as an average of the total electronic occupation for the two rhodiums of the second layer in the unit cell.

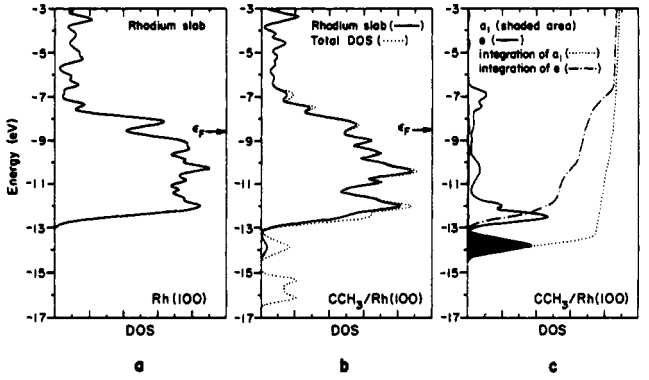

Figure 2. Some density of states plots for the clean Rh(100) surface and the 4-fold adsorbed ethylidyne surface. (a) Total DOS for a clean Rh(100) surface. (b) Rhodium slab contribution in the adsorbed system (solid line) and total DOS (dotted line). (c) Projected DOS for a_1 (shaded area) with integration of a_1 (dotted line) and projected DOS of e (solid line) with integration (– · –).

whereas the e orbitals gain ~1.75 electrons. These numbers are relative to the neutral fragment. The e orbitals must interact strongly with the surface, since after the adsorption they are only occupied by ~2.75 electrons. The rest of the states (1.25 electrons per ethylidyne) must be located above the Fermi level. This will be seen in the DOS plots. The calculated depletion of electron density in the surface Rh layer is, in principle, testable with X-ray photoemission spectroscopy, i.e., core level shifts.[31] No such measurements are as yet available.

Figure 2 shows some projected DOS for the clean Rh(100) surface and the 4-fold adsorbed system. The total DOS for the bare Rh(100) slab is depicted in Figure 2a. The peak between –8 and –13 ev consists mainly of rhodium 4d states. The states above the d block are the 5s and 5p orbitals of rhodium, though some penetration of these states into the d block region is calculated. The projected DOS for the rhodium slab in the adsorbed system is plotted in Figure 2b. A comparison with the clean surface reveals that some states have moved around. A new peak is found from –13 to –14.5 eV. The shape of the d block has also changed. Contributions of the frontier orbitals of ethylidyne to the DOS are seen in Figure 2c. The major part of a_1 (shaded area) is pushed down from –12.7 eV in free ethylidyne to ~–13.7 eV, coincident with the new peak in the DOS for the rhodium slab after adsorption. The integration curve for a_1 shows that some a_1 states are also found in the d block region. The e orbitals spread out to a rather wide band. A major peak is seen from –11.5 to –13 eV. Just above the Fermi level, around –7 eV, approximately 15% of the e states are found.

In order to trace the d orbitals involved in the interactions with a_1 and e, let us look at some projected DOS for the former. Figure 3 displays the orbitals in the σ part of the interaction, which involves the a_1 orbital from ethylidyne. At left is shown the contributions from d_{z^2} of a clean Rh(100) surface (Figure 3a) and of the adsorbed system (Figure 3b). The d_{xy} orbital is plotted in Figure 3d and 3e. In the middle is shown the projected DOS of the a_1 orbital in the adsorbed system. Both d_{z^2} and d_{xy} pick up density in the a_1 region of ~–13.7 eV. This indicates that an interaction is going on between a_1 and these two d orbitals. The a_1 orbital acts as a donor toward the metal surface, being stabilized itself by ~1 eV and pushing up the d orbitals with which it interacts. Indeed, the projected DOS of d_{z^2} and d_{xy} do reflect this feature, by having more states at higher energies in the adsorbed system than for the clean Rh(100) surface. For d_{xy}, the interaction with a_1 pushes some states above the Fermi level, explaining why what we think of as the acceptor orbital of this interaction can in fact suffer a net depletion of electron density—a loss of 0.19 electron is computed. The d_{z^2}–a_1 part of the σ interaction is weaker. Only ~3% of the d_{z^2} states are found in the a_1 peak, ~–13.7 eV (d_{xy} have ~7% of its states here). A loss of only 0.07 electron for d_{z^2} is calculated, meaning that some of the antibonding Rh–C orbitals are still found below the Fermi level. The main part of the σ bond originates then from the bonding part of the d_{xy}–a_1 interaction, 17.

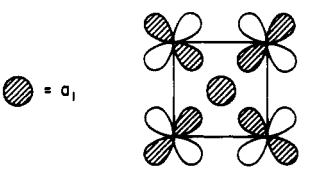

17

The π part of the surface–adsorbate bond can be analyzed in a similar way. The projected DOS of the orbitals involved are depicted in Figure 4. The two panels to the left show the projected DOS of the d_{xz} and d_{yz} orbitals of the clean (Figure 4a) and the ethylidyne-covered (Figure 4b) Rh(100) surface. The $d_{x^2-y^2}$ contributions are outlined at the right of the figure. In the central panel is shown the projected DOS of e. Notice that density is built up in the DOS plots for $d_{xz} + d_{yz}$ and $d_{x^2-y^2}$ around the energies of the two characteristic e peaks, at ~–7 and ~–12.5 eV, when ethylidyne is adsorbed. This is

(31) See: Shustorovich, E. M., Baetzold, R. *Science* **1985**, *227*, 876.

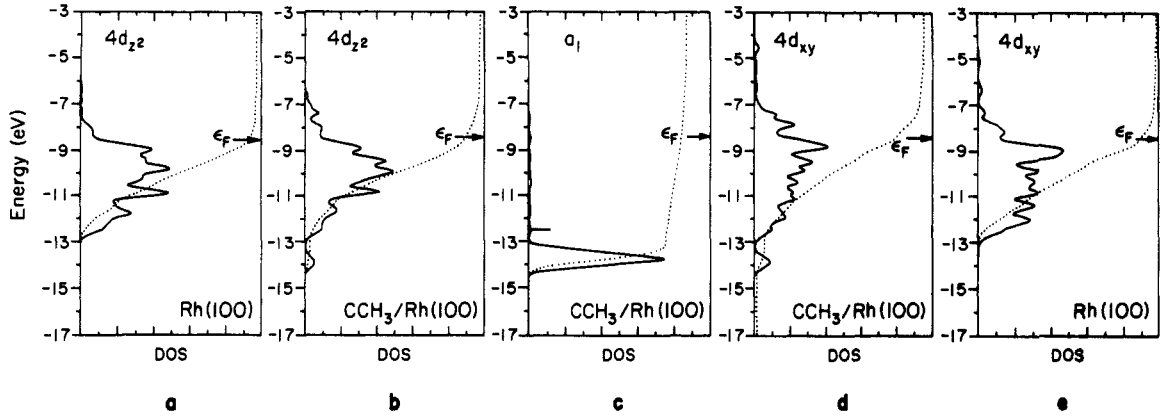

Figure 3. Density of states projections (solid lines) illustrating the σ interaction between a 4-fold adsorbed ethylidyne and the Rh(100) surface. (a) d_{z^2} for the clean Rh(100) surface. (b) d_{z^2} for the adsorbed system. (c) a_1 for the adsorbed system. (d) Rhodium d_{xy} orbital when interacting with ethylidyne. (e) d_{xy} orbital for a clean Rh(100) surface. The horizontal stick in c represents the energy of a_1 in free ethylidyne. Dotted lines give integrations of the projected orbitals.

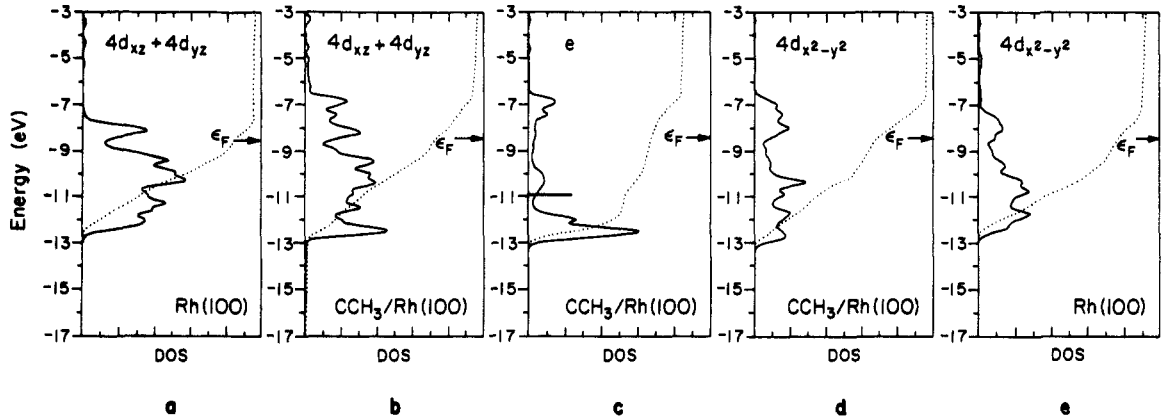

Figure 4. Projected density of states (solid lines) illustrating the π part of the surface adsorbate bond for 4-fold adsorbed ethylidyne on a Rh(100) surface. (a) $d_{xz} + d_{yz}$ for the clean Rh(100) surface. (b) $d_{xz} + d_{yz}$ for the adsorbed system. (c) e's for the adsorbed system. (d) Contribution from $d_{x^2-y^2}$ in the adsorbed system. (e) $d_{x^2-y^2}$ orbital for a clean Rh(100) surface. The horizontal stick in c represents the energy of e in free ethylidyne. Dotted lines give integrations of the projected orbitals.

strong indication of an interaction going on. The e orbitals are excellent π acceptor orbitals, because of their very low energy compared with the Fermi level of Rh(100). A loss of 0.47 electron is calculated for the $d_{xz} + d_{yz}$ orbitals, and another 0.18 electron is lost from $d_{x^2-y^2}$. Some of the resulting bonding orbitals are drawn in 18.

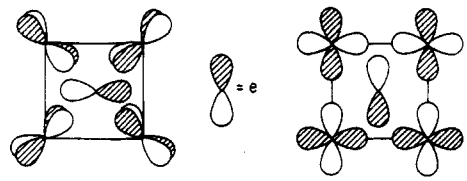

18

An examination of the COOP curves in Figure 5 for the 4-fold adsorbed system supports these conclusions. Figure 5a is the COOP curve for the surface Rh–C bond. Figure 5b shows COOP curves for the carbon–carbon bond and for the carbon–hydrogen bonds of ethylidyne. The Rh–C bond is composed of orbitals around −13.7 and −12.5 eV. The former peak corresponds to the σ interactions of a_1 with d_{xy} and d_{z^2}, and the latter peak is the π part of the bond. The COOPs of Figure 5b provide some further evidence. The orbitals located around −13.7 eV are C–C bonding and weakly C–H bonding, as expected from the shape of the a_1 orbital. No orbitals other than e of ethylidyne have C–C antibonding character together with a C–H bonding feature, such as Figure 5b shows the −12.5-eV peak has. From the COOPs it can be concluded that the surface–ethylidyne bond is dominated by the π component, because the π peak in Figure 5a is significantly larger than the σ peak. This conclusion is supported by an analysis of the individual band contributions to the overlap population.

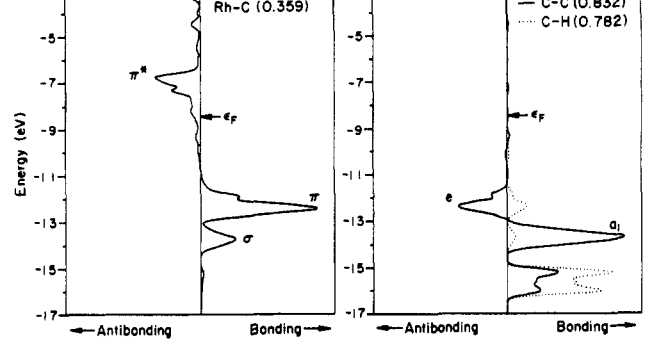

Figure 5. COOP plots for the 4-fold ethylidyne covered Rh(100) surface. (a) Surface rhodium to carbon bond. (b) COOPs for the C–C bond (solid line) and the C–H bonds (dotted line). Numbers in the legend indicate the total overlap population.

As indicated by the DOS plots, the antibonding part of the π interaction is found around −7 eV. This should also be reflected in the C–C and C–H COOPs in Figure 5b. But neither C-C nor C–H bonding characteristics show up at this energy. A second-order mixing of the 2e

orbitals of ethylidyne into e accounts for this, at first glance, strange feature. The 2e orbital is strongly C–C and C–H antibonding, **19**.

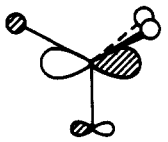

19

The $2p_x$ and $2p_y$ atomic orbitals of the methyl carbon have large coefficients in 2e, in contrast to the e orbitals. Let us analyze how a second-order mixing of 2e into e in the −7-eV region can explain the lack of C–C and C–H bonding or antibonding character, by splitting the interaction into two sequential first-order mixings.[32] The process is illustrated schematically in **20**. First we mix e with surface d orbitals. The e orbitals are lower in energy than the d orbitals. The bonding component of the interaction will be composed mainly of e with some d character mixed into it. This is found at ~−12.5 eV. The antibonding counterpart will consist of d orbitals with e mixed in out-of-phase, as drawn at the top right of **20**.

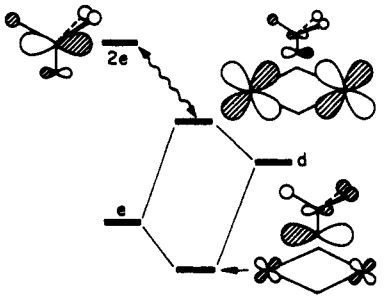

20

We now mix 2e into the antibonding combination. The phase with which 2e mixes in will be controlled by the 2e–d interaction, because the d orbitals are the major contributors to the orbital in question. The d orbitals are located lower in energy than 2e; hence 2e will mix in a Rh–C bonding way: the phase is as shown in **21** (λ is an MO mixing coefficient). The net result is that in the primarily d-type orbital the 2p coefficients on the methyl carbon contributed by e and 2e, through their respective interactions, cancel.

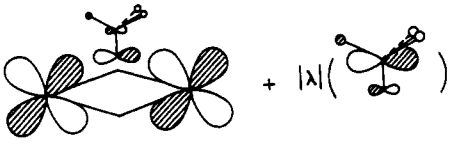

21

In Figure 6 the DOS for 2e is projected out. It does pick up density in the range of interest around −7 eV. The mixing of 2e is rather small. Only about ~0.01 electron is donated from the metal to 2e. But in this −7-eV region, the extent of mixing is exactly enough to cancel out any p orbital contribution from the methyl carbon. Another indication of this e–2e mixing is seen in Figure 2c. All e states are not seen in this window, but the integration line shows that ~15% of the states are to be found above −3 eV.

(32) Libit, L.; Hoffmann, R. *J. Am. Chem. Soc.* **1974**, *96*, 1370.

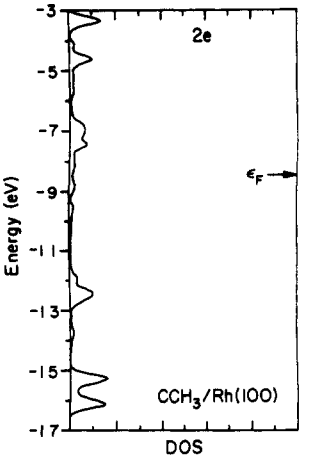

Figure 6. Magnified projected density of states for 2e in the 4-fold adsorbed geometry.

Let us go on to a comparison with the other adsorption sites of Rh(100) and with the 3-fold adsorption on Rh(111). The adsorption process for these three sites can be analyzed in a similar way as just done for the 4-fold adsorbed surface. We will not go into any detailed analysis for these sites will but only outline the most important interactions found. **22** shows those interactions for on-top adsorption, where the surface adsorbate bond is composed of a σ donation from a_1 to d_{z^2}, **22a**, and a π back-bonding from d_{xz} and d_{yz} to e, **22b**.

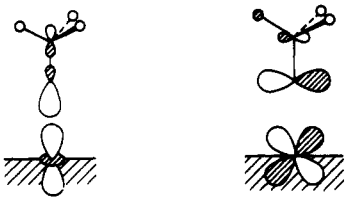

22

Upon going to more bridging sites, more d orbitals get involved. The most important interactions in the 2-fold bridging structure are shown in **23**. The interactions between the (111) surface of an fcc metal and a 3-fold hollow site adsorbed ethylidyne have been investigated in an earlier report from our group.[18] The bonding interactions for this structure are outlined in **24**.

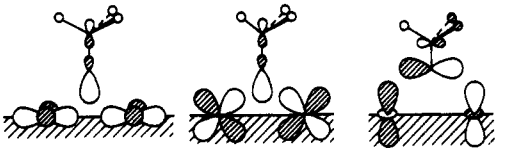

23

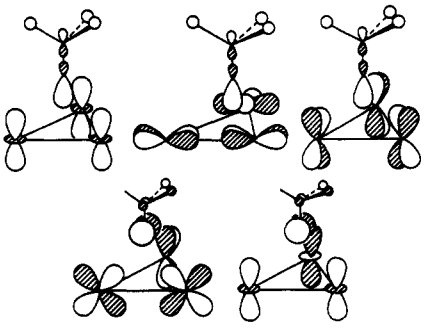

24

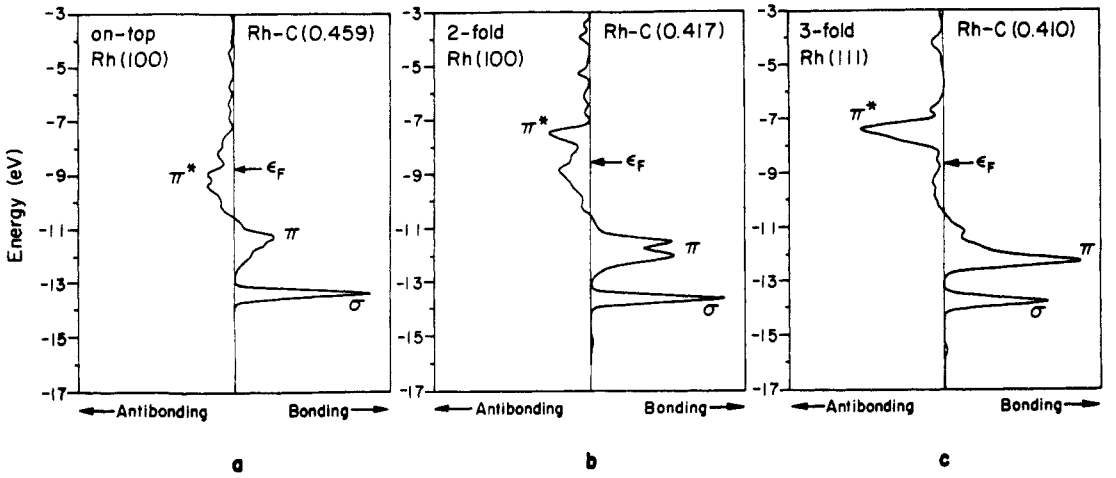

Figure 7. COOP curves for the surface rhodium to carbon bond in the different geometries. (a) Ethylidyne adsorbed in the on-top position of the Rh(100) surface. (b) Bridging ethylidyne on Rh(100). (c) A 3-fold adsorbed ethylidyne on Rh(111). The numbers in the legend are the total overlap populations.

Table III. Electron Densities for the a_1 and e Orbitals of Adsorbed Ethylidyne on Rh(100) and Rh(111)

orbital	on-top Rh(100)	2-fold Rh(100)	4-fold Rh(100)	3-fold Rh(111)
a_1	1.69	1.68	1.69	1.64
e	3.85	3.46	2.75	2.95

Table IV. Equilibrium Rh–C Distances,[a] Changes in C–C Equilibrium Distance,[b] and Binding Energies[c] for Ethylidyne on Different Rh(111) and (100) Sites

property	on-top	2-fold	3-fold/4-fold
(111)			
R_e(Rh–C)	1.81	1.96	2.04
ΔR_e(C–C)	−0.01	0.0	0.01
ΔE_{MO}	6.4	6.8	7.2
ΔE	4.4	5.0	5.5
(100)			
R_e(Rh–C)	1.81	1.94	2.12[d]
ΔR_e(C–C)	0.0	0.0	−0.01
ΔE_{MO}	6.4	7.2	7.3
ΔE	4.5	5.3	5.9

[a] R_e(Rh–C), Å. [b] R_e(C–C), Å. [c] ΔE, eV. [d] 4-fold.

Calculated electron densities of the frontier orbitals of ethylidyne are listed in Table III. In all four sites investigated, the a_1 orbital acts as a donor, donating ~0.3 electron to the surface. The major difference between the sites is to be found in the occupation of the e level. The on-top site has the largest occupation of 3.85 electrons, whereas only 2.75 electrons occupy e in the 4-fold adsorbed structure. A less occupied e orbital means a stronger C–C bond, due to the antibonding C–C character of this orbital. This is reflected in the C–C overlap populations listed in Table I (the C–C overlap population for a 3-fold adsorbed ethylidyne on Rh(111) is 0.821).

The preference of the 4-fold hollow site on Rh(100) and the 3-fold hollow site on Rh(111) is also seen in the Rh–C overlap populations. They are given in Table I for adsorption on Rh(100). The comparison is between four populations of 0.359 in the 4-fold site versus two of 0.417 in the 2-fold bridging site and one of 0.459 in the on-top site. The earlier analysis with CCH_3 on Pt(111)[18] gave the same trend, with the highest single metal carbon overlap population in the on-top site. Calculations for ethylidyne on Rh(111) reproduce this trend; in the on-top site there is one bond with an overlap population of 0.439 and in the 3-fold site three of 0.410.

The extent of interaction of e with the d band and the position of the Fermi level are behind this trend. The e level and corresponding d orbitals interact more or less strongly, giving bonding and antibonding combinations. One easy way to follow this is through the Rh–C COOP curves. These are shown in Figure 7 for on-top (Figure 7a) and 2-fold bridging (Figure 7b) adsorption on Rh(100). The Rh–C COOP for the 4-fold adsorbed ethylidyne was plotted in Figure 5a. Figure 7c shows the same bond for the 3-fold adsorbed Rh(111) system. Note the peaks marked π and π^*. They are split in the sequence 4-fold > 3-fold > 2-fold > on-top, and this in turn is a consequence of the group–orbital overlaps behind the interactions.[33] The Fermi level, set largely by the bulk, does not change much between the adsorption sites. And it falls so that in the on-top case many Rh–C antibonding states are filled (see Figure 7a), less so in the 2-fold bridging and 3-fold bridging sites. The fewest Rh–C antibonding states are filled in the most stable 4-fold hollow site. Along with the stronger π bond, it should be noticed that the relative intensity of the π peak compared with the s peak increases on going to more bridging sites, which indicates that the π bonding is more important in the bridging sites.[34]

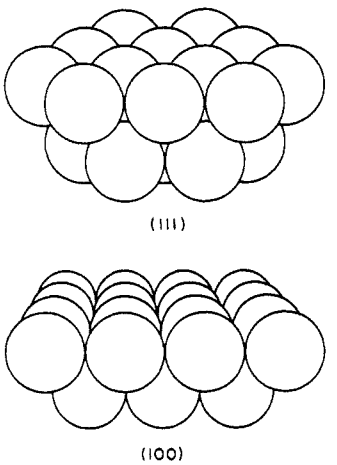

Figure 8. Rh_{19} and Rh_{25} cluster models of the (111) and (100) surfaces used in the ASED-MO calculations. CCH_3 binding is studied over the three top central atoms of the Rh_{19} cluster and over the four top central atoms of the Rh_{25} cluster.

(33) For examples of how the group orbitals can be traced in various surface–adsorbate systems, see for instance: Van Santen, R. A. *J. Chem. Soc., Faraday Trans. 1* **1987**, *83*, 1915. Zonnevylle, M. C.; Hoffmann, R.; van den Hoek, P. J.; van Santen, R. A. To be published.

Table V. Extended Hückel Atomic and ASED-MO Parameters[a]

atom	orbital	H_{ii}, eV	ζ_1	ζ_2	c_1[b]	c_2[b]
Rh	5s	-7.31	2.13			
		(-8.46)	(2.135)			
	5p	-3.39	2.10			
		(-5.10)	(1.835)			
	4d	-10.35	4.29	1.97	0.5807	0.5685
		(-10.56)	(5.542)	(2.098)	(0.5823)	(0.6405)
Cr	4s	-8.66	1.70			
	4p	-5.24	1.70			
	3d	-11.20	4.95	1.80	0.5058	0.6747
Ru	5s	-9.37	2.08			
	5p	-4.35	2.04			
	4d	-12.33	5.38	2.30	0.5342	0.6368
Cl	3s	-26.30	2.183			
	3p	-14.20	1.733			
O	2s	-32.20	2.275			
	2p	-14.80	2.275			
C	2s	-21.40	1.63			
		(-15.59)	(1.658)			
	2p	-11.40	1.63			
		(-10.26)	(1.618)			
H	1s	-13.60	1.30			
		(-12.60)	(1.20)			

[a] ASED-MO parameters in parentheses. [b] Coefficients used in the double-ζ expansion of the metal d-orbitals.

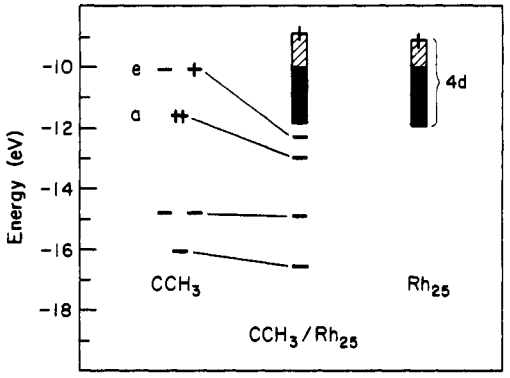

Figure 9. Stabilizations of e and a orbitals of CCH_3 when bound on the 4-fold site of the Rh_{25} cluster model of the (100) surface as determined by the ASED-MO calculations. Solid regions of the metal band indicate doubly occupied orbitals, and cross-hatched regions indicate half-filled orbitals in accordance with the spin polarization rule assumed in ASED-MO calculations that each d band orbital is occupied by at least one electron.

As a final comment, it should be mentioned that calculations were done for other C_s geometries of the CCH_3/Rh(100) system. In these geometries, ethylidyne sits in sites in between the high-symmetry sites. The calculations for these sites give results that also are in between the values obtained for the on-top, 2-fold bridging and 4-fold hollow sites.

ASED-MO Results for Ethylidyne on Rh(111) and (100)

The atom superposition and electron delocalization molecular orbital (ASED-MO) method combines an extended Hückel-like electron delocalization molecular orbital energy, E_{MO}, with pairwise repulsive energy components, E_R, from atom superposition. The binding energy is thus given as $\Delta E = \Delta E_{MO} + \Delta E_R$, and from this energy, structures and force constants can be calculated. Two-layer-thick Rh_{19} and Rh_{25} cluster models are used for the (111) and (100) surfaces, respectively. They are shown in Figure 8. Atomic parameters are based on literature values with C and H VSIP decreased by 1 eV and Rh VSIP increased by 1 eV to reduce metal–hydrocarbon charge transfer as was done in the Pt studies.[9d,14]

As Table IV shows, the 3-fold site is favored for ethylidyne on Rh(111), and the Rh–C distance in this site is 2.04 Å, agreeing with the 2.03 Å experimental experimental value.[11a] The C–C bond stretches slightly on going from the low- to high-coordination sites of Rh(111).

On the (100) surface, the 4-fold site is favored, with a Rh–C distance of 2.12 Å. Adsorption is a bit stronger than on the (111) surface. This time the C–C bond shrinks slightly on going from the low- to high-coordination sites. The correlation diagram of Figure 9 for CCH_3 in the 4-fold site clearly shows the covalent and charge-transfer stabilizations. Their description is essentially the same as given above for the extended Hückel tight-binding results.

Over both surface models, the Rh–C equilibrium distance is predicted to decrease as the degree of coordination to the metal decreases. This is a typical result and may be attributed to the reduction in number of pairwise two-body repulsion energy components on going to lower coordination. The extended Hückel calculations, by assuming the same Rh–C distances for all coordinations, have compensated for the lack of two-body repulsion energy components, so that both approaches yield the same site preference and about the same adsorption energies for CCH_3 on these surfaces.

Conclusions

In agreement with the experimental results, both sets of calculations make the 4-fold site the most likely place for ethylidyne to sit on the Rh(100) surface. This is from an energetic point of view as well as from a bonding analysis. The bond between the surface and a 4-fold adsorbed ethylidyne fragment consists of a σ part, where a_1 donates electrons to the metal, and a π part, through back-bonding to the e orbitals. The surface has no problems providing the appropriate orbitals for that back-bonding.

From a bonding analysis, the 4-fold site is preferred, because the π interaction in this geometry is very strong. This is indicated by the appearance of the π^* peak above the Fermi level. A consequence of this strong interac-

(34) It is a general trend that strong π accepting adsorbates prefer to sit in the most coordinated site of the surface. For a study of CH on various surfaces, see: Zheng, C.; Apeloig, Y.; Hoffmann, R. *J. Am. Chem. Soc.* **1988**, *110*, 749. For PF on Ni(111), see: Chan, A. W. E.; Hoffmann, R. To be published.

tion is partly filled e orbitals and a stronger C–C bond, as reflected by the large C–C overlap population calculated for this site. Even in comparison with the well-characterized 3-fold adsorbed Rh(111) system, the 4-fold site of Rh(100) does very well, even better if we judge by the C–C overlap population. The stretching frequencies show the opposite trend, the highest one being for 3-fold adsorbed ethylidyne. The ASED-MO CC bond length predictions also oppose this trend. While the effects of coupling C–C, M–C, and C–H modes need to be investigated to try to resolve these contradictions, it may be that both theoretical methods are at fault. High-accuracy SCF calculations would be interesting.

Acknowledgment. B.S. is thankful to the Carlsberg Foundation and Thanks To Scandinavia, Inc. (especially Richard Netter), who have made her stay at Cornell possible. B.S. also thanks Jing Li for helpful discussions. The Cornell effort was supported by the Office of Naval Research and the work at Case-Western Reserve University by the Gas Research Institute. M.K.A. is grateful to Tanta University for granting leave and to the Government of Egypt for graduate fellowship support. We are grateful to Jane Jorgensen and Elisabeth Fields for their expert drawings.

Appendix

For the extended Hückel tight-binding calculations the Rh–C bond distance is kept at 2.20 Å in all geometries. The C–C distance is 1.45 Å, and C–H is taken to be 1.10 Å in all calculations. The rhodium parameters are taken from ref 35, and the ruthenium H_{ii}'s are obtained from a charge iteration on the parent compound to **2**, $Ru_2(CO)_2(Cp)_2(\mu^2\text{-}CO)_2$,[36] with *A*, *B*, and *C* parameters taken from ref 37. Atomic parameters are summarized in Table IV. For the calculation of properties averaged over the Brillouin zone, a 16K point set was used for the Rh(100) geometries and a 9K point set was used for the Rh(111) structures according to the geometrical method by Ramirez and Böhm.[38]

Registry No. CCH_3, 67624-57-1; Rh, 7440-16-6.

(35) Vuckovic, D. Lj.; Jansen, S.; Hoffman, R. To be published.
(36) Mills, O. S.; Nice, J. P. *J. Organomet. Chem.* **1967**, *9*, 339.
(37) Baranovskii, V. I.; Nikolskii, A. B. *Teor, Eksp. Khim.* **1967**, *3*, 527.
(38) Ramirez, R.; Böhm, M. C. *Int. Quantum. Chem.* **1986**, *30*, 391.

A Mechanistic Study of the Oxidative Addition Reaction of Benzyl Thiocyanate at Iron, Nickel, and Zinc Surfaces in Sulfuric Acid

Tetsuya Suzuki, Hiroshi Nishihara,* and Kunitsugu Aramaki

Department of Chemistry, Faculty of Science and Technology, Keio University, Hiyoshi 3-14-1, Yokohama 223, Japan

Received August 14, 1989. In Final Form: November 16, 1989

Reactions of benzyl thiocyanate at Fe, Ni, and Zn surfaces in sulfuric acid were studied in relation to the corrosion inhibition behavior of benzyl thiocyanate. Corrosion inhibition efficiency obtained by the electrochemical polarization method was extremely high for Fe and Ni but modest for Zn. Benzyl thiocyanate decomposed at these three metal surfaces, and the decay kinetics, which was first order in benzyl thiocyanate, was slow on Fe and Ni but fast on Zn. Formation of a multiple-layer film on the metals was indicated from the amount of benzyl thiocyanate consumed when the metals contact with the benzyl thiocyanate solution. Thiocyanate ion, benzaldehyde, toluene, and benzyl mercaptan were detected as the reaction products. Benzaldehyde was mainly formed on Fe and Ni, while toluene and benzyl mercaptan were the major products on Zn. Conclusions on the reaction mechanism deduced from these results are as follows: oxidative addition of benzyl thiocyanate to the surface metal atoms forms a multiple-layer film on the surface which is resistive against the metal corrosion; the reaction products on Fe and Ni consist of an η^3-benzyl–metal π-binding, whereas the product on Zn is composed of an η^1-benzyl–Zn σ-bonding; and the high stability of the π-bonding of benzyl ligand with Fe and Ni gives the excellent corrosion protection ability.

Introduction

"Oxidative addition" expresses the reaction where a group, A–B, adds to, and thus oxidizes, a metal or metal complex, M, to form A–M–B, A–M+B$^-$, M–A + M–B, or A–M–M–B. This reaction has been extensively studied in organometallic chemistry.[1-4] Especially, the oxidative addition to low-valent transition-metal complexes has been attracting much attention, since this reaction is involved in a variety of homogeneous catalytic reaction processes.[5] As for the oxidative addition reactions on transition-metal surfaces, gas-phase reactions have been much studied by the metal atom synthesis technique.[3,4] On the contrary, oxidative addition reactions occurring at the transition metal–solution interface have not been a subject of intensive studies, whereas the reactions on main group metals in solution such as Grignard reac-

(1) Still, J. K. In *The Chemistry of the Metal-Carbon Bond*; Hartley, F. R., Patai, S., Eds., Wiley: Chichester, 1985; Vol. 2, p 625.
(2) Collman, J. P.; Hegedus, L. S. *Principles and Applications of Organotransition Metal Chemistry*; University Science Books: Mill Valley, CA, 1980, Chapter 4.
(3) Timms, P. L.; Turney, T. W. *Adv. Organomet. Chem.* **1976**, *15*, 53.
(4) Klabunde, K. J. *Acc. Chem. Res.* **1975**, *8*, 393.
(5) Kochi, J. K. *Organometallic Mechanisms and Catalysis*; Academic Press: New York, 1978.

0743-7463/90/2406-0816$02.50/0